



Using potential field derivatives in the arctangent function to estimate the edges and relative depths of potential field sources

Yasin Nasuti¹, Luan Thanh Pham^{2*}

1. Department of Earth Sciences, Institute for Advanced Studies in Basic Sciences (IASBS), Zanjan 45137-66731, Iran.

2. Faculty of Physics, University of Science, Vietnam National University, Hanoi, Vietnam.

* Corresponding author: luanpt@hus.edu.vn

ABSTRACT

Several filtering methods have been introduced to estimate the edges of potential field sources. The selection of the appropriate technique depends on the type of data and the target. Among filtering techniques, phase-based filters are the most widely used methods due to the flexibility of their design, but they do not provide information on the source depth. In this study, some novel filtering approaches are proposed, highlighting the edge of adjacent sources with different intensities by initially removing the regional anomalies. These approaches generate low amplitude anomalies over the deep sources, and higher amplitude anomalies over the shallow sources, providing information on relative depths of the sources. To evaluate the designed approaches, synthetic and real data from the Finnmark area of North Norway were used. The results were compared with those obtained from other approaches. These results showed that the proposed approaches considerably simplify the interpretation of the anomaly maps with higher efficiency and broader interpretation scope than the classical techniques.

Keywords: Edge; depth; filter; potential field sources

Uso de derivadas de campos potenciales en la función inversa de la tangente para estimar los límites y las profundidades relativas de fuentes de campos potenciales

RESUMEN

Varios métodos de filtrado se han presentado para estimar los límites de las fuentes de campos potenciales. La selección de la técnica apropiada depende del tipo de información y del objetivo. Entre las técnicas de filtrado, los filtros de fase son los más usados debido a la flexibilidad de su diseño, sin embargo estos no proveen la profundidad de la fuente. En este estudio se propuso el acercamiento a algunos filtros novedosos, donde se resaltaron los límites de las fuentes adyacentes con diferentes intensidades al remover inicialmente las anomalías regionales. Estos métodos generaron anomalías de baja amplitud sobre las fuentes profundas y anomalías de mayor amplitud sobre las fuentes a poca profundidad, lo que provee información de las profundidades relativas de las fuentes. Para evaluar los modelos diseñados se usaron datos sintéticos y reales del área de Finnmark, en el norte de Noruega. Los resultados se compararon con valores obtenidos a través de otros métodos. Estos resultados muestran que los métodos propuestos simplifican considerablemente la interpretación de los mapas de anomalías con mayor eficiencia y en un alcance más amplio que las técnicas clásicas.

Palabras clave: Limite; profundidad; filtrado; fuentes de campos potenciales.

Record

Manuscript received: 07/10/2023

Accepted for publication: 18/09/2024

How to cite item:

Nasuti, Y., & Pham, L.T. (2024). Using potential field derivatives in the arctangent function to estimate the edges and relative depths of potential field sources. *Earth Sciences Research Journal*, 28(3), 265-276. <https://doi.org/10.15446/esrj.v28n3.111479>

1. Introduction

The potential field methods play an important role in mapping geological structures, particularly for mineral exploration (Eyjen, 1936; Cordell and Grauch, 1985; Dwivedi and Chamoli, 2022; Dwivedi et al., 2023; Kamto et al., 2023). Many filters of potential field data have been developed to estimate the source location (Nabighian, 1972, 1974; Wijns et al., 2005; Cooper and Cowan, 2006; Oksum et al., 2021; Pham, 2023; Kafadar and Oksum, 2024). By highlighting the edges of anomalies with various depths and magnitudes, filtering aids in the identification of additional details in the possible field data maps (Ekinci and Yiğitbaş, 2012, 2015; Ekinci et al., 2013; Narayan et al., 2017, 2021; Eldosouky, 2019; Eldosouky et al., 2022; Sahoo et al., 2022a, b; Pham and Prasad, 2023; Niñez-Demarco et al., 2023; Liu et al., 2023; Ekwok et al., 2023; Pham et al., 2022, 2024a; Aprina et al., 2024). High-pass filters have been used in several studies to highlight the edges of anomalies (Cordell and Grauch, 1985; Roest et al., 1992; Blakey, 1995; Hsu et al., 1996; and Fedi and Florio, 2001). To filter potential field data using various techniques, efforts have been made to balance the trade-off between noise and signal in the filtered image (Cooper and Cowan, 2006).

The vertical derivative filter is one of the frequently employed filters to identify anomaly edges (Eyjen, 1936; Ma et al., 2014). Higher-order vertical derivatives can effectively enhance anomalies, but they amplify the noise in data. The vertical derivative filter is usually limited to orders of one and two. This method is preferred when anomaly variation throughout the survey area is uniform. In other words, this filter is not able to balance the map.

The total horizontal derivative filter is another commonly used method to detect edges. Cordell and Grauch (1985) showed that the peak of the total horizontal gravity or pseudo-gravity data can indicate the edges of anomalies. The drawback of this strategy is that it might produce diffuse edges, which prevent the filter from being able to tell where weak anomalies and strong anomalies meet at the border (Li et al., 2012; Ma, 2013).

Another filter commonly used is the analytical signal or total gradient, which generates bell-shaped anomalies above magnetic bodies. This filter was developed by Nabighian (1972, 1974) and Roest et al. (1992). According to Grauch and Cordell (1987), the analytical signal cannot simultaneously enhance deep and shallow anomalies. To address this issue and improve the definition of adjacent anomalies, Hsu et al. (1996, 1998) used an enhanced analytical signal, which is the n th-order vertical derivative of the analytical signal. The impact of noise can be amplified by using higher order derivatives, so this technique is typically restricted to the first and second order.

In the last three decades, phase filters have received significant attention due to their flexibility (Wijns et al., 2005; Cooper and Cowan, 2006; Stampolidis and Tsokas, 2012; Li et al., 2013; Arisoy and Dikmen, 2013; Ferreira et al., 2013; Cooper, 2014; Ma et al., 2014; Zhang et al., 2015; Yao et al., 2016; Nasuti and Nasuti, 2018; Nasuti et al., 2019; Melouah and Pham, 2021; Pham et al., 2022b). The first phase filter is the tilt angle filter introduced by Miller and Singh (1994). Using the tilt angle filter, the source edges are represented by the zero values. To make the interpretation of the tilt-angle data easier, Verduzco et al. (2004) introduced a total horizontal derivative of the tilt angle filter. As the depth of the sources rises, the performance of the tilt angle and its total horizontal derivative may suffer. Additionally, the total horizontal derivative of the tilt angle is sensitive to noise, which can affect the accuracy of the results (Cooper and Cowan, 2006; Li et al., 2012; Ferreira et al., 2013; Nasuti and Nasuti, 2018).

To detect the edges of potential field sources, Ferreira et al. (2013) used the total horizontal derivative in the tilt angle equation. This method not only normalizes both shallow and deep potential field anomalous sources but also detects the edges of anomalies with very high precision. However, in case the shallow and deep sources located close together this filter is not able to discriminate them and will lose its resolution considerably (Zhang et al., 2015; Yao et al., 2016; Nasuti et al., 2019).

Cooper (2014) introduced the tilt angle of the analytical signal amplitude as a means of reducing the dependence on the source magnetization vector direction. This filter is appropriate in cases where the data has a remanent magnetization or when we are not able to reduce to magnetic pole due to lack of sufficient information from the sources, so that it transfers the anomalies to the top of the sources. It also creates a much better balance than the analytical signal in the data. The efficiency of this filter is reduced for adjacent sources that

are located at a short distance from each other. Also, in cases where the ratio of depth to width of the source is high, the maximum of this filter is placed above the anomaly.

Zhang et al. (2015) suggested using the tilt angle of the first order vertical derivative of the total horizontal derivative to distinguish between nearby sources. This filter perfectly equalizes the severity of deep and shallow anomalies and anomalies with different amplitudes and gives sharper and more accurate edges than the TAHG and TAS filters. This filter is also more effective in cases where anomalies of different depths and amplitudes are adjacent.

The concept of edge detection is not limited to the methods given above. Recently, some authors have developed other methods to map the source edges (Dwivedi and Chamoli, 2021, 2023; Kafadar, 2022; Prasad et al., 2022a, b, c; Dandan et al., 2023; Ibraheem et al., 2023; Jorge et al., 2023; Li et al., 2023; Alvandi et al., 2023; Alvandi and Ardestani, 2023; Pham, 2024 a,b,c; Pham et al., 2024b; Ai et al., 2024). Although these methods can bring the edges with high resolution, they do not provide the relative depths of potential field sources.

In this article, some new methods are introduced considering the slight changes in the previous filtering techniques, providing much better efficiency than the previous strategies. The images obtained from the new methods show deep anomalies with low amplitude and shallow anomalies with high amplitude. This can be used to distinguish deep anomalies from shallow anomalies, resulting in a wider interpretation scope.

2. Methodology

By using vertical derivatives of the amplitude-based filters that provide maxima over the source edges in the arctangent function, novel filters are introduced from the following general relation:

$$\text{New}_{(\text{Filter})} = \tan^{-1} \left(\frac{G|h|}{\sqrt{G}} \right) \rightarrow G \geq 0, G < 0 \rightarrow \text{Removed} \quad (1)$$

where h is a correction factor that is used to make the dimension unifying. In other words, the use of the factor h to make Eq. (1) has mathematical significance. This factor is given by:

$$h = \frac{\text{Max}(\sqrt{G})}{\text{Max}(G)}, \quad (2)$$

and G is the vertical derivative of some edge filters such as the total horizontal derivative (THD, Cordell and Grauch, 1985), analytical signal (AS, Roest et al., 1992), and vertical derivative of THD (THV, Zhang et al., 2015) that are given by:

$$\text{THD} = \sqrt{\left(\frac{\partial f}{\partial x} \right)^2 + \left(\frac{\partial f}{\partial y} \right)^2}, \quad (3)$$

$$\text{AS} = \sqrt{\left(\frac{\partial f}{\partial x} \right)^2 + \left(\frac{\partial f}{\partial y} \right)^2 + \left(\frac{\partial f}{\partial z} \right)^2}, \quad (4)$$

$$\text{THV} = \frac{\partial \text{THD}}{\partial z}, \quad (5)$$

where f is potential field data. Since G functions produce positive maxima over the edges, removing negative G values is helpful in bringing sharper edges. The proposed methods can be considered as modifications of the previous methods, i.e., the tilt angle of the THD (TAHG, Ferreira et al., 2013), tilt angle of the AS (TAS, Cooper, 2014) and tilt angle of the (TTHV, Zhang et al., 2015):

$$\text{TAHG} = \tan^{-1} \frac{\frac{\partial \text{THD}}{\partial z}}{\sqrt{\left(\frac{\partial \text{THD}}{\partial x}\right)^2 + \left(\frac{\partial \text{THD}}{\partial y}\right)^2}} \quad (6)$$

$$\text{TAS} = \tan^{-1} \frac{\frac{\partial \text{AS}}{\partial z}}{\sqrt{\left(\frac{\partial \text{AS}}{\partial x}\right)^2 + \left(\frac{\partial \text{AS}}{\partial y}\right)^2}} \quad (7)$$

$$\text{THVH} = \tan^{-1} \frac{\frac{\partial \text{THV}}{\partial z}}{\sqrt{\left(\frac{\partial \text{THV}}{\partial x}\right)^2 + \left(\frac{\partial \text{THV}}{\partial y}\right)^2}} \quad (8)$$

Using the proposed methods, the edges of deep sources are shown by low amplitude signals, while the edges of shallow sources are related to high amplitude signals. This can be used to distinguish deep anomalies from shallow anomalies. In the following sections, we demonstrate the effectiveness of the proposed methods on theoretical examples and real data from the Finnmark area, northern Norway.

3. Synthetic examples

We conducted synthetic studies to evaluate the strengths and limitations of the proposed approaches in enhancing the edges of magnetic anomalies.

The first model consists of 17 bodies (Fig. 1a) with an inclination of 90° and declination of 0°, and their geometrical and geomagnetic parameters are listed in Table 1. Figure 1b displays the synthetic magnetic anomaly of the model. The results obtained from applying the TAHG, N_{TAHG} , TAS, N_{TAS} , THVH, and N_{THVH} filters to magnetic data of the first model are presented in Figure 1 (c)-(h). The TAHG filter (Fig. 1c) highlights the edges of deep and shallow bodies by balancing different anomalies. The N_{TAHG} filter (Fig. 1d) shows the edges similar to the TAHG filter, except that it shows the response of deep bodies with low amplitude and shallow bodies with high amplitude, and the field around the bodies is removed. As clearly seen, in addition to the edges of the bodies, the relative depth of the bodies can also be distinguished by different transformed anomalies for different depths. The TAS filter (Fig. 1e) shows the edges of anomalies with less accuracy and sharpness than the TAHG filter. Also, in cases where the ratio of width to depth of the body is low, the peaks of this filter are above the anomalous bodies instead of the edges (bodies 6, 7 and 17). In the N_{TAS} method (Fig. 1f), the deep and shallow bodies can be separated, but its accuracy is less than the N_{TAHG} filter. We can see that the response of the bodies with non-vertical dip (bodies 5 and 6) has a small displacement in the direction of the dip of the bodies (Fig. 1f). Therefore, the dip of the bodies can be estimated by comparing the result of this filter with those from other methods. The THVH filter (Fig. 1g) has the same results as the TAHG filter, except that the THVH filter shows more detail with better sharpness than the TAHG. The N_{THVH} filter (Fig. 1h) has almost the same results as the N_{TAHG} filter, but it brings sharper edges compared to the N_{TAHG} filter. By using this filter, one can easily determine the geometric shape and position of adjacent bodies. However, the N_{THVH} map is noisy and this is one of its most important drawbacks.

Table 1. Geometric and magnetic parameters of the magnetic sources of the synthetic model 1 in Figure 1 (Magnetic Field=48000 nT, Inclination=90° and Declination=0°).

Model Label	Depth (m)	Thickness (m)	Strike length (m)	Depth extent (m)	Magnetic susceptibility (SI)	Dip (deg)	Azimuth (deg)
P1	10	100	500	1000	0.02	90	0
P2	20	100	500	1000	0.02	90	-45
P3	30	100	500	1000	0.02	90	45
P4	10	100	400	600	0.02	90	0
P5	40	100	400	600	0.02	60	0
P6	60	100	400	600	0.02	45	0
P7	30	100	100	1000	0.02	90	0
P8	20	100	100	1000	0.02	90	0
P9	10	100	100	1000	0.02	90	0
P10	30	600	300	1000	0.02	90	0
P11	10	200	100	1000	0.01	90	0
P12	10	100	300	1000	0.01	90	0
P13	20	100	300	1000	-0.02	90	0
P14	30	100	300	1000	0.02	90	0
P15	10	50	800	1000	0.01	90	0
P16	20	50	800	1000	0.02	90	0
P17	30	50	800	1000	0.02	90	0

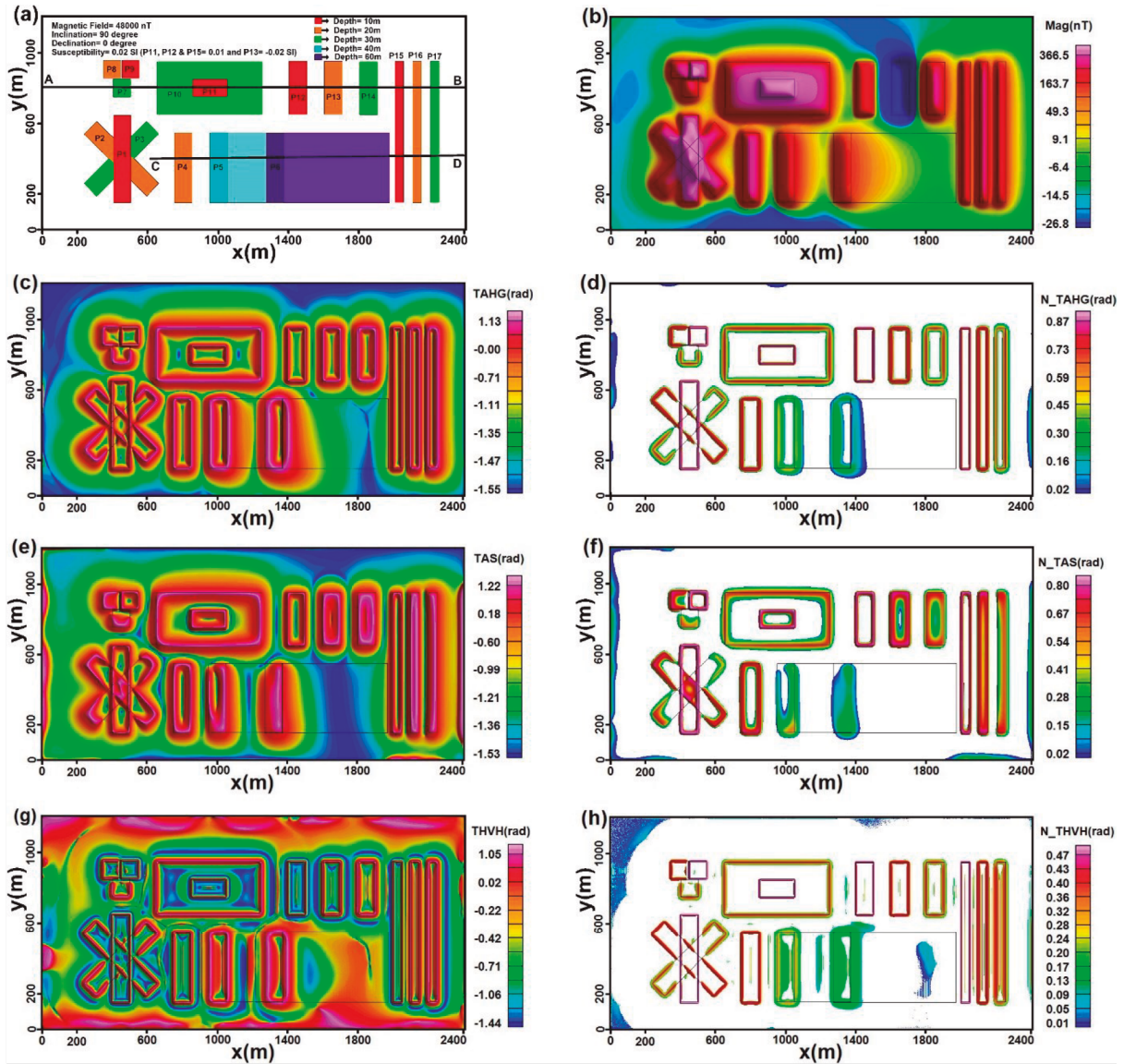


Figure 1. (a) Synthetic Model 1 indicating the location of the AB and CD profiles (see Figs. 2 and 3). (b) Magnetic anomaly of the model 1. (c) TAHG map. (d) N_{TAHG} map. (e) TAS map. (f) N_{TAS} map. (g) THVH map. (h) N_{THVH} map.

To aid in visualizing the quality of the above interpretations, Figures 2 and 3 show the results of the TAHG, N_{TAHG} , TAS, N_{TAS} , THVH, and N_{THVH} filters on the AB and CD profiles in Figure 1a. As can be seen, all the novel filters accurately show bodies of the same depth with the same intensity, while the commonly used filters provide the same intensity for all the bodies.

Analyzing magnetic anomalies can be challenging due to the influence of induced and remanent magnetization, which affects their shape. In this case, reducing the data to magnetic pole may not be possible. To estimate the efficacy of the proposed methods in this case, we consider the second synthetic model (Fig. 4a) with an inclination of -20° and a declination of -20° . The geometric and magnetic parameters of the bodies in this model are provided in Table 2, and the magnitude of the magnetic field is 28000nT. Figure 4b shows the magnetic

anomaly of the model. Figure 4 (c)-(h) show the results from applying the TAHG, N_{TAHG} , TAS, N_{TAS} , THVH, and N_{THVH} methods to magnetic data of the second model. As can be observed from these figures, the TAS and N_{TAS} filters (Figs. 4e and f) are much more efficient at determining the edge of anomalies than the other methods. The most important advantage of these filters is that they are less dependent on the direction of the magnetization vector than the other filters. Since the N_{TAS} values are dependent on the source depth, it can be used to estimate the relative depths of the bodies. Each of the new filters has disadvantages and advantages, therefore it is important to note that using 2 or 3 methods together improves the interpretation procedure by incorporating the advantages of each method.

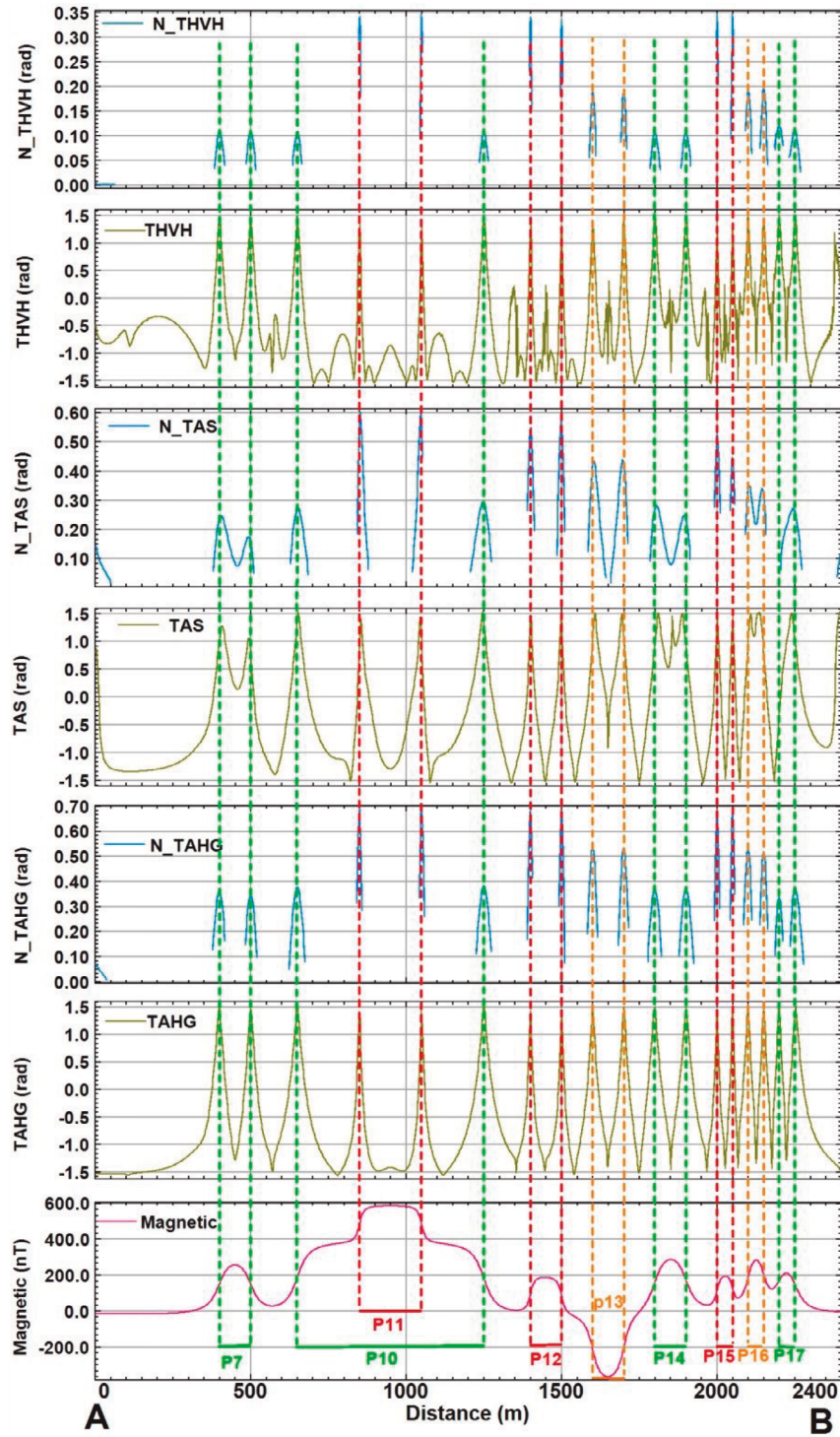


Figure 2. Profile AB constructed from synthetic model 1(see Fig. 1a).

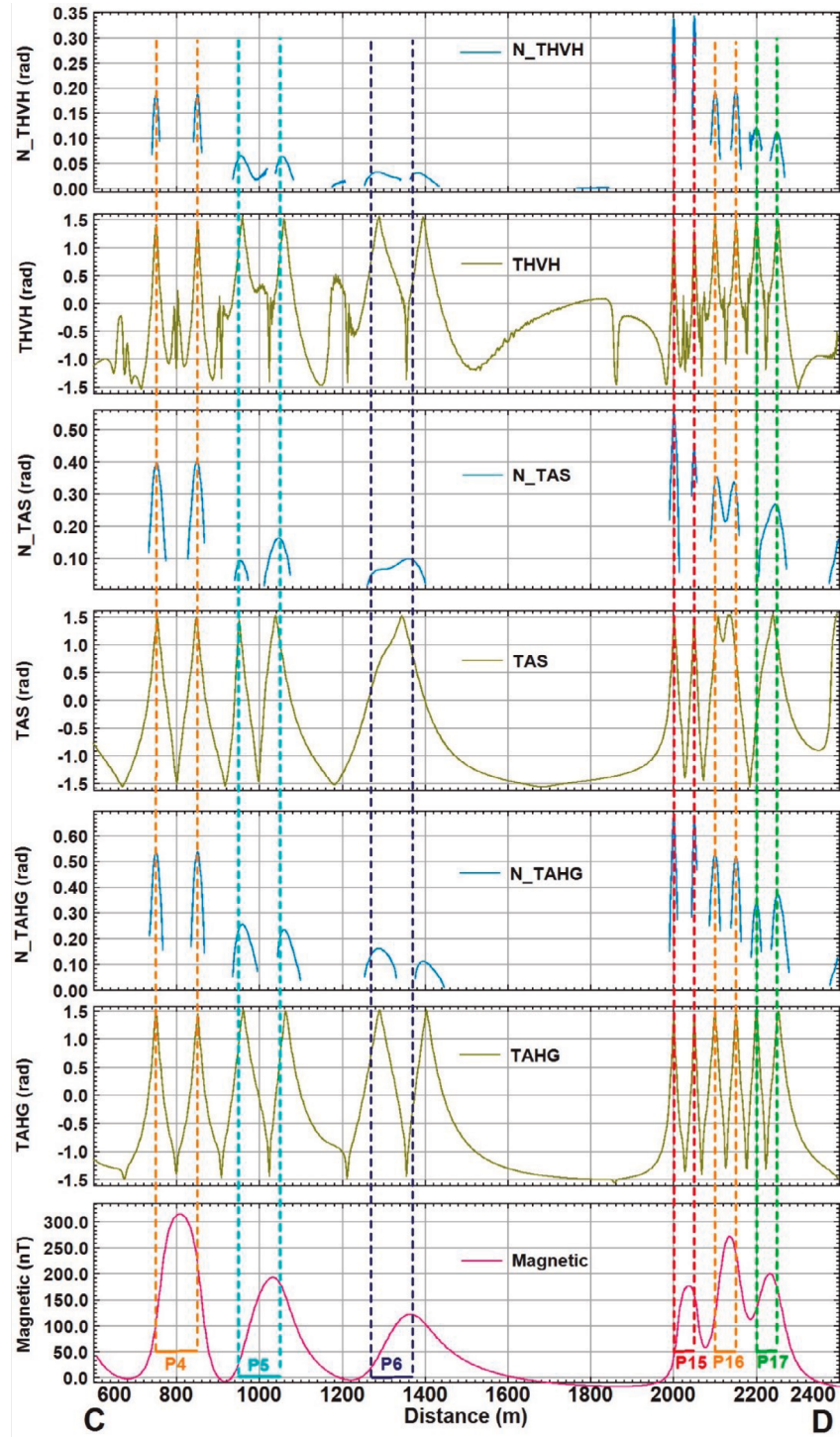


Figure 3. Profile CD constructed from synthetic model 1(see Fig. 1a).

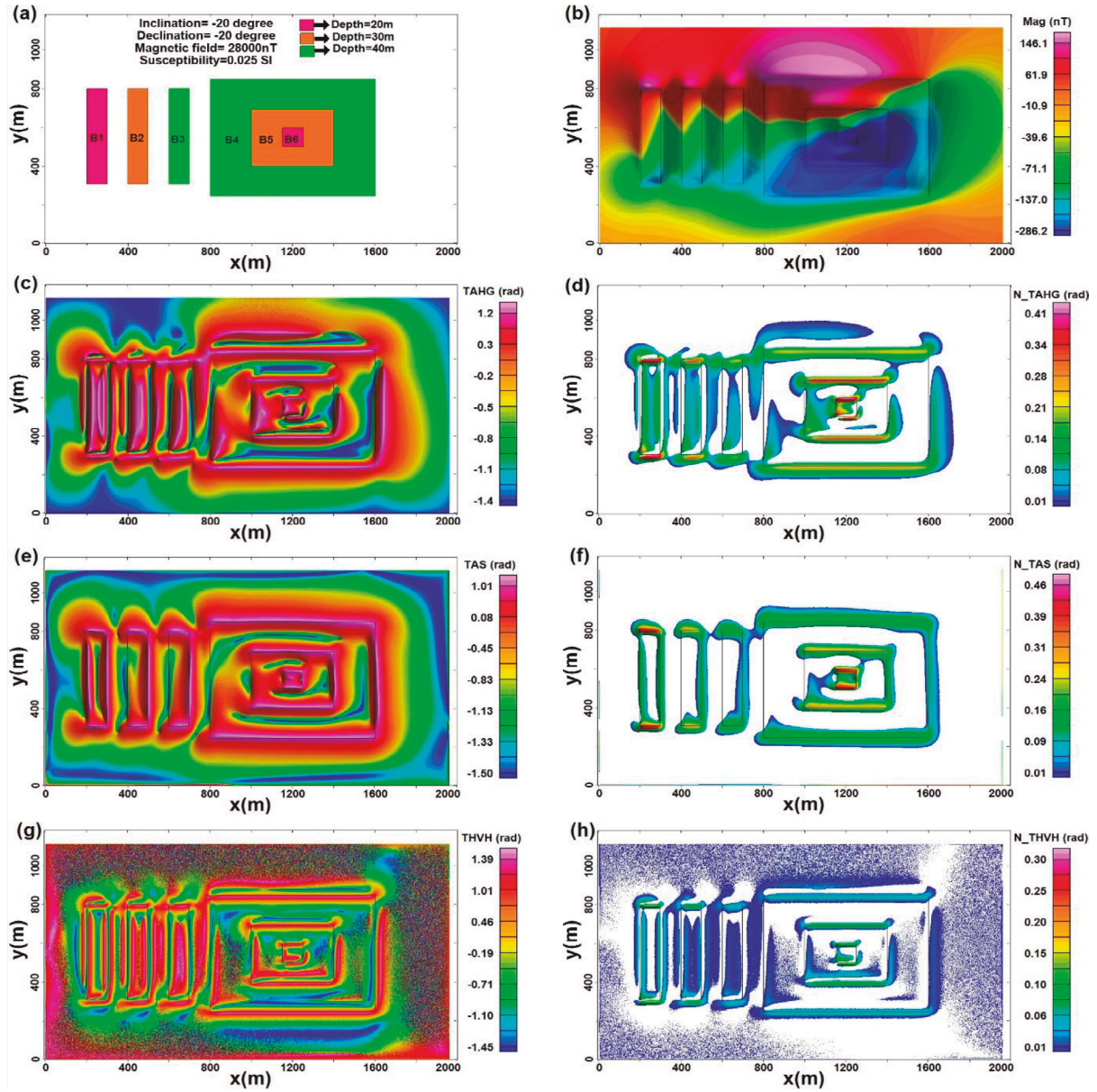


Figure 4. (a) Synthetic Model 2. (b) Magnetic anomaly of model 2. (c) TAHG map. (d) N_{TAHG} map. (e) TAS map. (f) N_{TAS} map. (g) THVH map. (h) N_{THVH} map.

Table 2. Geometric and magnetic parameters of the magnetic sources of the synthetic model 2 in Figure 5 (Magnetic Field=28000 nT, Inclination= -20° and Declination= -20°)

Model Label	Depth (m)	Thickness (m)	Strike length (m)	Depth extent (m)	Magnetic susceptibility (SI)	Dip (deg)	Azimuth (deg)
B1	20	100	500	1000	0.025	90	0
B2	30	100	500	1000	0.025	90	0
B3	40	100	500	1000	0.025	90	0
B4	40	800	600	1000	0.025	90	0
B5	20	400	300	1000	0.025	90	0
B6	30	100	100	1000	0.025	90	0

4. Application to magnetic data of the Finnmark area

To estimate the effectiveness of the proposed methods for real case scenarios, we applied them to interpret real data from the Finnmark area, North Norway (Fig. 5). The northern region of Norway (Fig. 5) is mainly composed of rock complexes formed during the Precambrian to Early Palaeozoic era. Most of these rock complexes were involved in the Caledonian orogeny to varying degrees. The bedrock geology can be broadly divided into two categories - the precise definition of the Caledonides and a mid-crustal continental lithospheric basement made up of native crystalline complexes that date from the Neoproterozoic to the Late Palaeoproterozoic. According to *Gaál et al. (1989)* and *Daly et al. (2006)*, these structures define the Fennoscandian Shield's northern boundary. Most of the ancient Precambrian rocks can be found in the western Troms and eastern Finnmark areas. These rocks include some that have undergone Caledonian action or have been incorporated into Caledonian Nappes (Fig. 5). Figure 6a shows the geological map of the area (modified from *Koistinen et al., 2001*). This map depicts the presence of Precambrian rocks that

are exposed in the southern part of the area and are dominated by the NW-SE trend. These rocks mainly include mafic to intermediate granulitic rocks and felsic to intermediate granulitic rocks. However, one of the Caledonian nappes (i.e., Gaissa Nappe Complex) obscures the Precambrian strata in the northern portion. In the middle of the study region, the Caledonian front thrust boundary is easily distinguishable.

To explore minerals, aeromagnetic measurements were carried out in the Finnmark area (highlighted by the yellow box in Fig. 5) from 2009 and 2014 with a flight line separation of 200 m (Novatem 2012, 2014; Nasuti et al., 2019). The flight height was generally from 60 m to 200 m (Nasuti et al., 2019). The average intensity of the Earth's magnetic field is 53600 nT. This selected area comprises adjacent deep and shallow anomalies, as well as anomalies of varying intensities. To reduce noise, the aeromagnetic data was upward-continued to 50 m before calculating the filters. Aeromagnetic anomalies were also reduced to the north magnetic pole using the inclination and declination angles of 78.5° and 10.6°, respectively. Figure 6b shows the reduction to the pole of upward-continued magnetic data.

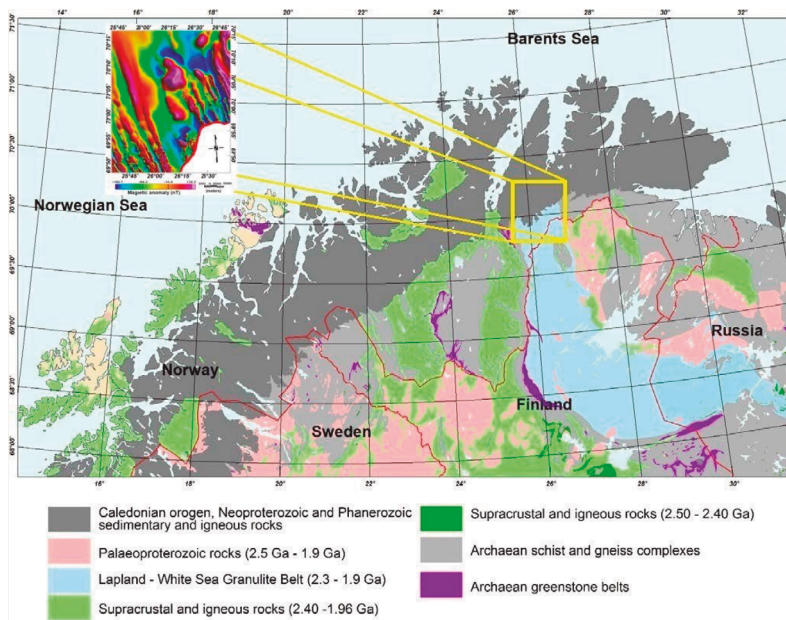


Figure 5. The tectonostratigraphic map of northern Scandinavia (modified from Koistinen et al., 2001), with the study area delimited by the yellow box.

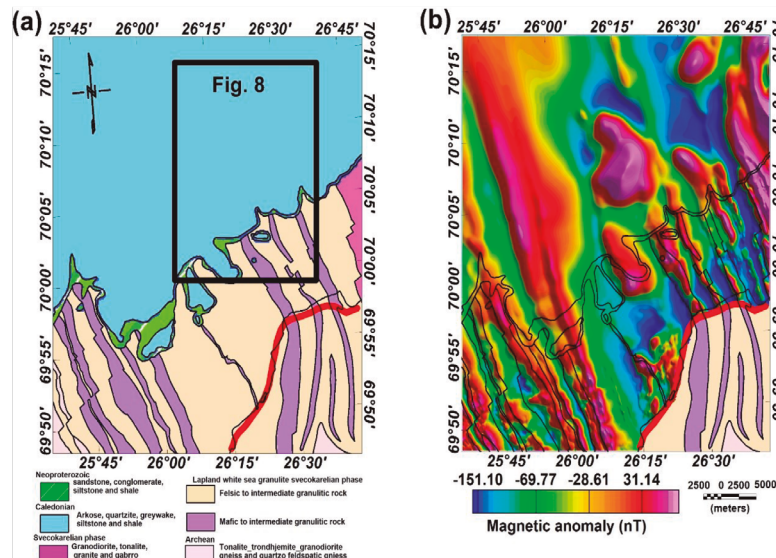


Figure 6. (a) Geological map of northern Norway. (b) Magnetic anomalies of the area.

The results from applying the TAHG, N_{TAHG} , TAS, N_{TAS} , THVH, and N_{THVH} filters to magnetic data in Figure 6b are displayed in Figure 7a-f. As can be observed, the proposed filters (Figs. 7b, d and f) allow for a clearer estimation of the edges in comparison with their counterparts (Figs. 7a, c and e). The new filters show deep anomalies with low amplitude and shallow anomalies with higher amplitude (rather than equally amplifying anomalies of different intensities and depths). In other words, the anomaly of the Precambrian layers (that are in the south to the center of the study area) is shown with a high amplitude and the anomaly of the other layers (that have gone from the center to the north of the region below Gaissa Nappe Complex) are presented with a low amplitude. The

Precambrian layers are located at a greater depth in this area, or the thickness of the Gaissa Nappe Complex above the Precambrian layers is greater in this area than in other areas. Therefore, by observing the range of anomalies in the maps obtained from the proposed filters (Figs. 7b, d and f), we can understand the relative depth of the sources and can realize the trend of structures and tectonics in the region. In other words, the images obtained from the proposed methods cover a wider range of interpretations. Among these techniques, the N_{THVH} map (Fig. 7f) has shown the range of deep and shallow anomalies with better accuracy, so that the boundary of Caledonian with Precambrian can be better defined compared to other methods (Figs. 7b and d).

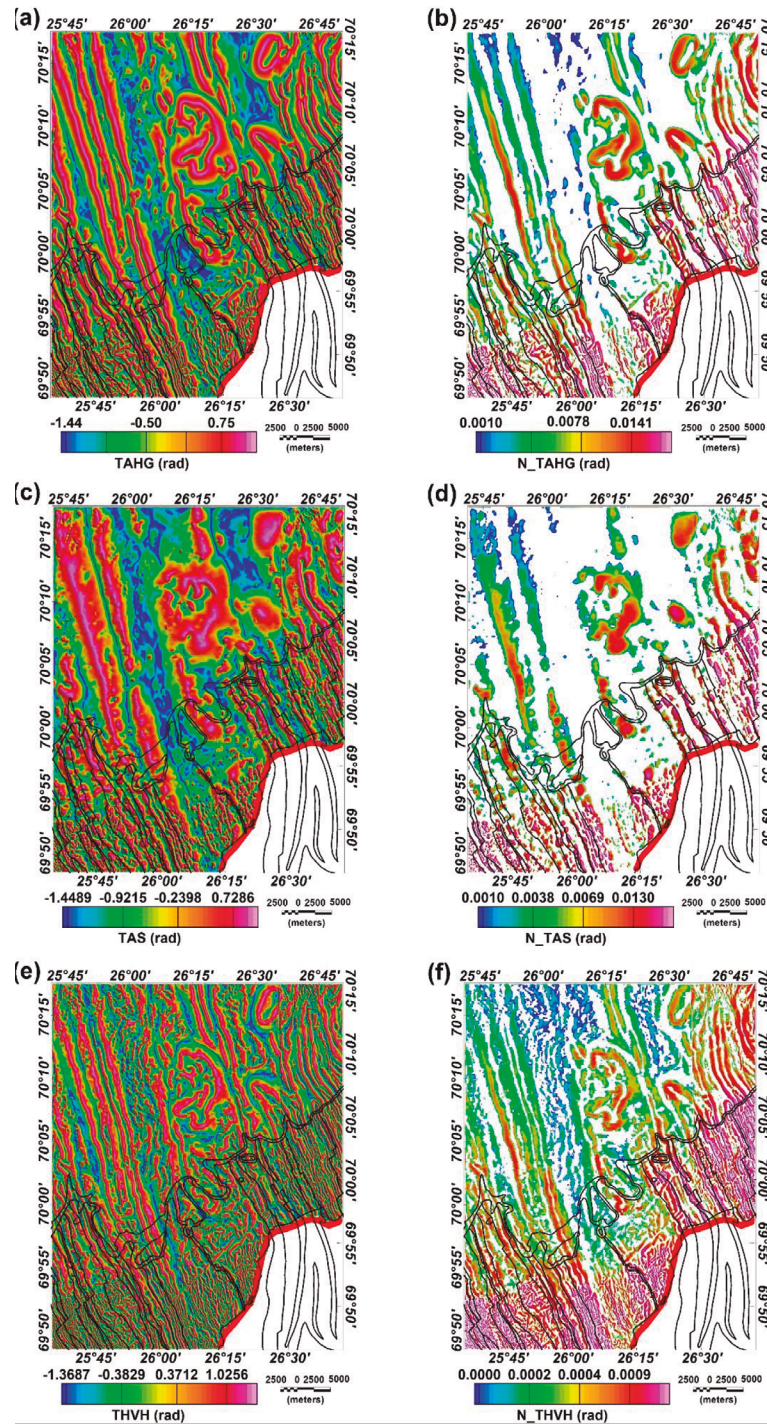


Figure 7. Application of different filters to high-resolution measured data from northern Norway. (a) TAHG map. (b) N_{TAHG} map. (c) TAS map. (d) NTAS map. (e) THVH map. (f) N_{THVH} map. Red line depicts the international border.

To further illustrate the strength of the filters, we selected a smaller area inside the black box shown in Figure 6a. Figure 8a shows the geological map of the study area, while Figure 8(b)-(d) exhibit the outcomes of the edge detection techniques, including N_{TAHG} , N_{TAS} , and N_{THVH} applied to magnetic data of this area. The N_{TAHG} and N_{THVH} filters offer high sharpness in detecting the source edges, while the N_{TAS} provide maxima over the sources. It was discovered that the N_{TAHG} and N_{THVH} filters were very successful in locating the extension of the Precambrian rocks beneath the Gaissa Nappe. Moreover, the N_{TAHG} and N_{THVH} filters also provided a clearer differentiation of the neighboring rock units. It is important to note that this approach not only improves the representation of structure continuity but also yields more lucid and organized visuals for the interpreter. Apart from the edges of the anomalies, our methods can estimate the relative depth of the magnetic structures in the area. As can be observed, the map of all the newly introduced methods (Figs. 8b, c and d) shows a decrease in the amplitude of anomalies related to the Precambrian layers from south to north, and the results obtained by these methods are highly compatible with each other.

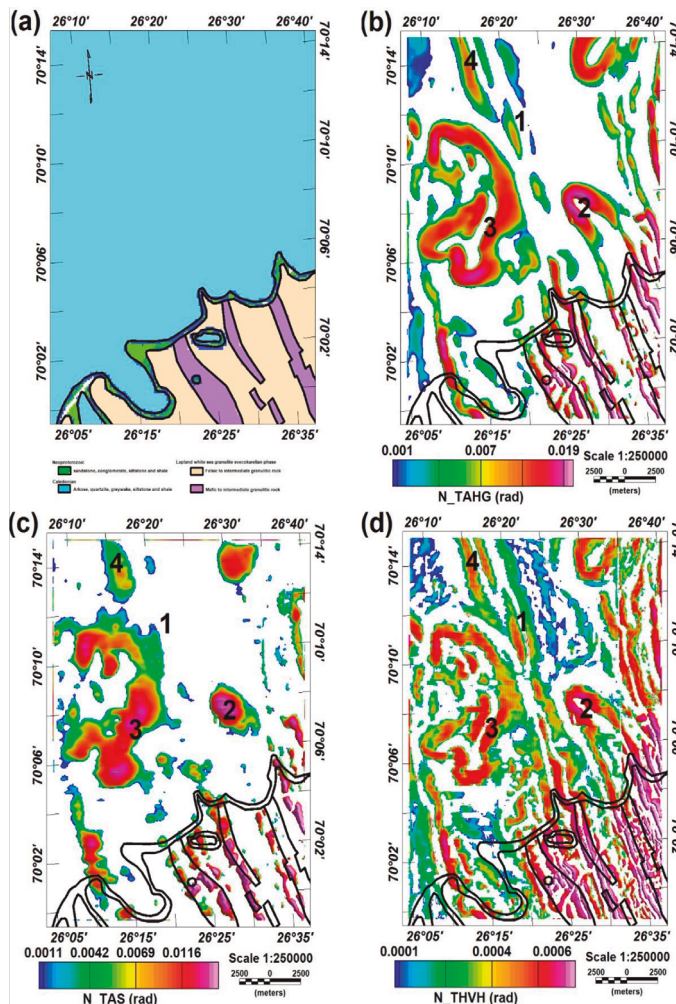


Figure 8. Application of the new methods on the selected area (see Fig. 6a for location). (a) Geological map of the area. (b) N_{TAHG} map. (c) N_{TAS} map. (d) N_{THVH} map. Labels 1, 2, 3 and 4 are four anomalies determined from applying the new methods.

To investigate the placement of the adjacent layers based on Figure 8b, we labeled four anomalies 1, 2, 3 and 4. The N_{TAHG} filter (Fig. 8b) does not show well the part of anomaly number one that is adjacent to anomalies 2 and 3. In the N_{THVH} map (Fig 8d), the source 1 is clear, but the N_{TAS} filter (Fig. 8c) does not provide any response to this source. From the high amplitude of bodies 2 and 3 in the N_{THVH} map, it can be said that the body 1 is deeper in this area than the bodies 2 and 3. Considering the location of the anomalies in the filter map and comparing it with other methods, it can be said that no magnetic remanent

is observed in these data. The geological map of the area also confirms this for the Precambrian layers that are exposed in the southern part of the area.

5. Conclusions

In this study, some novel filters have been introduced for interpretation of the potential field data. The proposed approaches highlight and separate the edges of adjacent anomalies with different intensities. The anomalies around the source edges are initially removed. The responses over the edges of the anomalies will remain where the low amplitude responses are related to the deep bodies, while the high amplitude responses show the shallow bodies. These results, therefore, also present the relative depth of the source bodies. The proposed filtering strategies simplify considerably the interpretation of the potential data and provide a wider interpretation scope. Theoretical simulations demonstrated a better performance of the novel methods for filtering potential data in comparison with the original methods. Moreover, the results from the application of these techniques to real data from North Norway are consistent with the known geological structures of the area. In the real example, the new methods also yielded clearer results compared to traditional methods.

Acknowledgements

The authors gratefully acknowledges Institute for Advanced Studies in Basic Sciences for supporting this project. We extend our gratitude to the reviewers for their constructive feedback, which greatly improved the manuscript. We further acknowledge Davood Moghadas, Hossein Fazli and Arya Farkhondeh for their valuable comments and assistance in refining the English language used in the manuscript.

References

- Ai, H., Deniz Toktay, H., Alvandi, A., Pašteka, R., Su, K., & Liu, Q. (2024). Advancing potential field data analysis: the Modified Horizontal Gradient Amplitude method (MHGA). *Contributions to Geophysics and Geodesy*, 54(2), 119-143. <https://doi.org/10.31577/congeo.2024.54.2.1>
- Alvandi, A., & Ardestani V. E. (2023). Edge detection of potential field anomalies using the Gompertz function as a high-resolution edge enhancement filter. *Bull Geophys Oceanogr*, 64 (3), 279-300. <https://doi.org/10.4430/bgo00420>
- Alvandi, A., Su, K., Ai, H., Ardestani, V. E., & Lyu, C. (2023). Enhancement of potential field source boundaries using the hyperbolic domain (Gudermannian function). *Minerals*, 13, 10, 1312. <https://doi.org/10.3390/min13101312>
- Aprina, P. U., Santoso, D., Alawiyah, S., Prasetyo, N., & Ibrahim, K. (2024). Delineating geological structure utilizing integration of remote sensing and gravity data: a study from Halmahera, North Molucca, Indonesia. *Vietnam J. Earth Sci.*, 46, 2, 147-168. <https://doi.org/10.15625/2615-9783/20010>
- Arisoy, M. Ö., & Dikmen, Ü. (2013). Edge detection of magnetic sources using enhanced total horizontal derivative of the tilt angle. *Yerbilimleri*, 34(1), 73-82.
- Bingen, B., Solli, A., Viola, G., Torgersen, E., Sandstad, J. S., Whitehouse, M. J., & Nasuti, A. (2015). Geochronology of the Palaeoproterozoic Kautokeino Greenstone Belt, Finnmark, Norway: Tectonic implications in a Fennoscandia context. *Norwegian Journal of Geology*, 95, 365-396. <http://dx.doi.org/10.17850/njg95-3-09>
- Blakely, R. J. (1995). *Potential theory in gravity and magnetic applications*. Cambridge University Press. <https://doi.org/10.1017/CBO9780511549816>
- Chamoli, A., Rana, S. K., Divyanshu, D., & Pandey, A. K. (2023). Crustal structure and fault geometries of the Garhwal Himalaya, India: Insight from new high-resolution gravity data modeling and PSO inversion. *Tectonophysics*, 859, 229904. <https://doi.org/10.1016/j.tecto.2023.229904>
- Cooper G. R. J., 2014. Reducing the dependence of the analytic signal amplitude of aeromagnetic data on the source vector direction. *Geophysics*, 79(4), J55-J60. <https://doi.org/10.1190/geo2013-0319.1>

- Cooper, G. R. J., & Cowan, D. R. (2006). Enhancing potential field data using filters based on the local phase. *Computers & Geosciences*, 32(10), 1585-1591. <https://doi.org/10.1016/j.cageo.2006.02.016>
- Cordell, L., & Grauch, V. J. S. (1985). Mapping basement magnetization zones from aeromagnetic data in the San Juan basin, New Mexico. In: Hinz, W. J. (Ed.). *The utility of regional gravity and magnetic anomaly maps*. Society of Exploration Geophysicists, 181-197. <https://doi.org/10.1190/1.0931830346.ch16>
- Daly, J.S., Balagansky, V. V., Timmerman, M. J., & Whitehouse, M. J. (2006). The Lapland-Kola orogen: Palaeoproterozoic collision and accretion of the northern Fennoscandian lithosphere. *Geological Society, London, Memoirs*, 32(1), 579-598. <https://doi.org/10.1144/GSL.MEM.2006.032.01.35>
- Dandan J., Qi, Z. & Hairong Z. (2023). A new method of balanced edge detection based on curvature for gravity data. *Acta Geophys.*, <https://doi.org/10.1007/s11600-022-00995-1>
- Dwivedi, D., & Chamoli, A. (2021). Source Edge Detection of Potential Field Data Using Wavelet Decomposition. *Pure Appl. Geophys.*, 178, 919–938. <https://doi.org/10.1007/s00024-021-02675-5>
- Dwivedi D., & Chamoli A., 2022. Seismotectonics and lineament fabric of Delhi fold belt region, India. *J. Earth Syst. Sci.*, 131, 74. <https://doi.org/10.1007/s12040-022-01829-w>.
- Dwivedi, D., Chamoli, A., & Rana, S.K. (2023). Wavelet Entropy: A New Tool for Edge Detection of Potential Field Data. *Entropy*, 25, 240. <https://doi.org/10.3390/e25020240>
- Ekinci, Y. L., Ertekin, C., & Yigitbas, E. (2013) On the effectiveness of directional derivative based filters on gravity anomalies for source edge approximation: synthetic simulations and a case study from the Aegean graben system (western Anatolia, Turkey). *J Geophys Eng.*, 10(3), 035005. <https://doi.org/10.1088/1742-2132/10/3/035005>
- Ekinci, Y. L., & Yigitbas E. (2012). A geophysical approach to the igneous rocks in the Biga Peninsula (NW Turkey) based on airborne magnetic anomalies: Geological implications. *Geodin Acta*, 25, 267–285. <https://doi.org/10.1080/09853111.2013.858945>
- Ekinci, Y. L., & Yigitbas, E. (2015). Interpretation of gravity anomalies to delineate some structural features of Biga and Gelibolu peninsulas, and their surroundings (northwest Turkey). *Geodinam Acta*, 27(4), 300–319. <https://doi.org/10.1080/09853111.2015.1046354>
- Ekwok, S. E., Eldosouky, A. M., Ben, U. C., Achadu, O. I. M., Akpan, A. E., Othman, A., & Pham, L. T. (2023). An integrated approach of advanced methods for mapping geologic structures and sedimentary thickness in Ukelle and adjoining region (Southeast Nigeria). *Earth Sciences Research Journal*, 27(3), 251-258. <https://doi.org/10.15446/esrj.v27n3.105868>
- Eldosouky, A. M. (2019). Aeromagnetic data for mapping geologic contacts at Samr El-qaa area, North Eastern Desert, Egypt. *Arabian Journal of Geosciences*, 12, 2. <https://doi.org/10.1007/s12517-018-4182-2>
- Eldosouky, A. M., Ekwok, S. E., Akpan, A. E., Achadu, O. I. M., Pham, L. T., Abdelrahman, K., Gómez-Ortiz, D., & Alarif, S. S. (2022). Delineation of structural lineaments of Southeast Nigeria using high resolution aeromagnetic data. *Open Geosciences*, 14, 331–340. <https://doi.org/10.1515/geo-2022-0360>
- EON Geosciences Inc., 2015. *Troms-Finmark fixed wing aeromagnetic survey 2014 (TROFI-14)*. Report EON Geosciences Inc., Montréal, Quebec, Canada, 34 pp
- Evjen, H. M. (1936). The place of the vertical gradient in gravitational interpretations. *Geophysics*, 1(1), 127-136. <https://doi.org/10.1190/1.1437067>
- Fedi, M., & Florio, G. (2001). Detection of potential fields source boundaries by enhanced horizontal derivative method. *Geophysical Prospecting*, 49(1), 40–58. <https://doi.org/10.1046/j.1365-2478.2001.00235.x>
- Ferreira, F. J. F., de Souza, J., de B. e S. Bongiolo, A., & de Castro, L. G. (2013). Enhancement of the total horizontal gradient of magnetic anomalies using the tilt angle. *Geophysics*, 78(3), J33–J41. <https://doi.org/10.1190/geo2011-0441.1>
- Gaal G., Berthelsen A., Gorbatshev R., Kesola R., Lehtonen M. I., Marker M. & Raase P., 1989. Structure and composition of the Precambrian crust along the POLAR Profile in the northern Baltic Shield. *Tectonophysics*, 162(1-2), 1-25. [https://doi.org/10.1016/0040-1951\(89\)90354-5](https://doi.org/10.1016/0040-1951(89)90354-5)
- Geologian tutkimuskeskus (Finland), Kaistinen T., Stephens M. B., & Bogatchev V., 2001. *Geological map of the Fennoscandian Shield*. Geological Survey of Finland.
- Grauch V.J.S. & Cordell L., 1987. Limitations of determining density or magnetic boundaries from the horizontal gradient of gravity or pseudogravity data. *Geophysics*, 52(1), 118-121. <https://doi.org/10.1190/1.1442236>
- Henderson I.H., Viola G. & Nasuti A., 2015. A new tectonic model for the Palaeoproterozoic Kautokeino Greenstone Belt, northern Norway, based on high-resolution airborne magnetic data and field structural analysis and implications for mineral potential. *Norwegian Journal of Geology*, 95(3-4), 339-364. <http://dx.doi.org/10.17850/njg95-3-05>
- Hsu S.K., Sibuet J.C. & Shyu C.T., 1996. High-resolution detection of geologic boundaries from potential-field anomalies: An enhanced analytic signal technique. *Geophysics*, 61(2), 373-386. <http://dx.doi.org/10.1190/1.1443966>
- Ibraheem I.M., Tezkan B., Ghazala H. & Othman A.A., 2023. A New Edge Enhancement Filter for the Interpretation of Magnetic Field Data. *Pure and Applied Geophysics*, <https://doi.org/10.1007/s00024-023-03249-3>.
- Jorge, V. T., Oliveira, S. P., Pham L. T., & Duong, V. H. (2023). A balanced edge detector for aeromagnetic data. *Vietnam Journal of Earth Sciences*, 43(3), 326–337. <https://doi.org/10.15625/2615-9783/18461>
- Kamto, P. G., Oksum, E., Pham, L. T., & Kamguia, J. (2023). Contribution of advanced edge detection filters for the structural mapping of the Douala Sedimentary Basin along the Gulf of Guinea. *Vietnam Journal of Earth Sciences*, 43(3), 287–302. <https://doi.org/10.15625/2615-9783/18410>
- Kafadar O., 2022. Applications of the Kuwahara and Gaussian filters on potential field data. *J Appl Geophys*, 198, 104583. <https://doi.org/10.1016/j.jappgeo.2022.104583>
- Kafadar O., & Oksum E., 2024. Enhanced dip angle map using Kuwahara and Gaussian filters: an example from Burdur region, Türkiye. *Turk. J. Earth Sci.*, 33(4), 395-406. <https://doi.org/10.55730/1300-0985.1919>
- Li L., Ma G. & Du X., 2013. Edge detection in potential-field data by enhanced mathematical morphology filter. *Pure and Applied Geophysics*, 170(4), 645-653. <https://doi.org/10.1007/s00024-012-0545-x>
- Li G., Liu S., Shi K., & Hu X., 2023. Normalized Edge Detectors Using Full Gradient Tensors of Potential Field. *Pure Appl. Geophys.* <https://doi.org/10.1007/s00024-023-03274-2>
- Liu J, Li S, Jiang S, Wang X. & Zhang J., 2023. Tools for Edge Detection of Gravity Data: Comparison and Application to Tectonic Boundary Mapping in the Molucca Sea. *Surv Geophys.* <https://doi.org/10.1007/s10712-023-09784-x>
- Ma G., 2013. Edge detection of potential field data using improved local phase filter. *Exploration Geophysics*, 44(1), 36-41. <https://doi.org/10.1071/EG12022>
- Ma G., Liu C. & Li L., 2014. Balanced horizontal derivative of potential field data to recognize the edges and estimate location parameters of the source. *Journal of Applied Geophysics*, 108, 12-18. <https://doi.org/10.1016/j.jappgeo.2014.06.005>
- Melouah O. & Pham L.T., 2021. An improved ILTHG method for edge enhancement of geological structures: application to gravity data from the Oued Righ valley. *Journal of African Earth Sciences*, 177, 104162. <https://doi.org/10.1016/j.jafrearsci.2021.104162>
- Miller H. G. & Singh V., 1994. Potential field tilt—a new concept for location of potential field sources. *Journal of applied Geophysics*, 32(2-3), 213-217. [https://doi.org/10.1016/0926-9851\(94\)90022-1](https://doi.org/10.1016/0926-9851(94)90022-1)

- Nabighian M.N., 1972. The analytic signal of two-dimensional magnetic bodies with polygonal cross-section: its properties and use for automated anomaly interpretation. *Geophysics*, 37(3), 507-517. <https://doi.org/10.1190/1.1440276>
- Nabighian M.N., 1974. Additional comments on the analytic signal of two-dimensional magnetic bodies with polygonal cross-section. *Geophysics*, 39(1), 85-92. <https://doi.org/10.1190/1.1440416>
- Narayan, S., Sahoo, S.D., Pal, S.K., Kumar, U., Pathak, V.K., Majumdar, T.J., & Chouhan, A., 2017. Delineation of structural features over a part of the Bay of Bengal using total and balanced horizontal derivative techniques. *Geocarto Int.*, 32 (4), 351–366. <http://dx.doi.org/10.1080/10106049.2016.1140823>
- Narayan S., Kumar U., Pal S.K. & Sahoo S.D., 2021. New insights into the structural and tectonic settings of the Bay of Bengal using high-resolution earth gravity model data. *Acta Geophys*, 69, 2011–2033. <https://doi.org/10.1007/s11600-021-00657-8>
- Nasuti Y. & Nasuti A., 2018. NTilt as an improved enhanced tilt derivative filter for edge detection of potential field anomalies. *Geophysical Journal International*, 214(1), 36-45. <https://doi.org/10.1093/gji/ggy117>
- Nasuti Y., Nasuti A. & Moghadas D., 2019. STDR: A novel approach for enhancing and edge detection of potential field data. *Pure and Applied Geophysics*, 176(2), 827-841. <https://doi.org/10.1007/s00024-018-2016-5>
- Novateme., 2012. *Fixed wing magnetic and radiometric survey of the coastal area of Northwestern Norway (FRAS-E)*. Report no. C11089, Novateme Airborne Geophysics, Mont-Saint Hilaire, Quebec, Canada, 36 pp.
- Novateme., 2014. *Fixed wing magnetic and radiometric survey over the Troms-Finnmark region in Northern Norway (TROFI-14 E)*. Report no. C14104, Novateme Airborne Geophysics, Mont-Saint Hilaire, Quebec, Canada, 29 pp.
- Núñez-Demarcó P., Bonilla A., Sánchez-Bettucci L., & Prezzi C., 2023. Potential-Field Filters for Gravity and Magnetic Interpretation: A Review. *Surv Geophys* 44, 603–664. <https://doi.org/10.1007/s10712-022-09752-x>
- Oksum E., Le D.V., Vu M.D., Nguyen T.H.T., & Pham L.T., 2021. A novel approach based on the fast sigmoid function for interpretation of potential field data. *Bull. Geophys. Oceanogr.* 62(3), 543–556. <https://doi.org/10.4430/bgta0348>
- Olesen O., & Sandstad J.S., 1993. Interpretation of the Proterozoic Kautokeino Greenstone Belt, Finnmark, Norway from combined geophysical and geological data. *Norges geologiske undersøkelse Bulletin*, 425, 41-62.
- Pham, L. T. (2023). A novel approach for enhancing potential fields: application to aeromagnetic data of the Tuangiao, Vietnam. *Eur. Phys. J. Plus*, 138 (12), 1134. <https://doi.org/10.1140/epjp/s13360-023-04760-1>
- Pham, L. T. (2024a). A stable method for detecting the edges of potential field sources. *IEEE Trans. Geosci. Remote Sens.* 62, 5912107. <https://doi.org/10.1109/TGRS.2024.3388294>
- Pham, L. T. (2024b). An improved edge detector for interpreting potential field data. *Earth Sci. Inform.*, 17, 2763-2774. <https://doi.org/10.1007/s12145-024-01286-7>
- Pham, L. T. (2024c). A new technique based on the eigenvalue of the curvature tensor for enhancing gravity data. *Annals Of Geophysics*, 67, 2, DM213. <https://doi.org/doi:10.4401/ag-9050>
- Pham, L. T., Oksum, E., Kafadar, O., Trinh, P. T., Nguyen, D. V., Vo, Q. T., Le, S. T., & Do, T. D. (2022). Determination of subsurface lineaments in the Hoang Sa islands using enhanced methods of gravity total horizontal gradient. *Vietnam Journal of Earth Sciences*, 44(3), 395-409. <https://doi.org/10.15625/2615-9783/17013>
- Pham, L.T, Oliveira, S.P, Le-Huy, M., Nguyen, D.V, Nguyen-Dang, T.Q, Do, T.D, Tran, K.V, Nguyen, H-D.T, Ngo, T-N.T, & Pham, H.Q (2024a). Reliable Euler deconvolution solutions of gravity data throughout the β -VDR and THGED methods: Application to mineral exploration and geological structural mapping. *Vietnam Journal of Earth Sciences*, 46(3), 432–448. <https://doi.org/10.15625/2615-9783/21009>
- Pham L.T, Abdelrahman K, Nguyen D.V, Gomez-Ortiz D., Long N.N, Luu L.D., Do T.D., Vo Q.T., Nguyen T-H.T, Nguyen H-D.T., & Eldosouky A.M. (2024b). Enhancement of the balanced total horizontal derivative of gravity data using the power law approach. *Geocarto International*, 39:1, 2335251, <https://doi.org/10.1080/10106049.2024.2335251>.
- Pham, L. T., & Prasad, K. N. D. (2023). Analysis of gravity data for extracting structural features of the northern region of the Central Indian Ridge. *Vietnam Journal of Earth Sciences*, <https://doi.org/10.15625/2615-9783/18206>
- Prasad, K. N. D., Pham, L. T., & Singh, A. P. (2022a). Structural mapping of potential field sources using BHG filter. *Geocarto Int.* 1–28. <https://doi.org/10.1080/10106049.2022.2048903>
- Prasad, K. N. D., Pham, L. T., & Singh, A. P. (2022b). A novel filter “ImpTAHG” for edge detection and a case study from Cambay Rift Basin, India. *Pure Appl Geophys.* 179(6-7), 2351–2364. <https://doi.org/10.1007/s00024-022-03059-z>.
- Prasad, K. N. D., Pham, L. T., & Singh, A. P. Eldosouky, A. M., Abdelrahman, K., Fnais, M. S., & Gómez-Ortiz, D. (2022c). A Novel Enhanced Total Gradient (ETG) for Interpretation of Magnetic Data. *Minerals*, 12, 1468. <https://doi.org/10.3390/min12111468>
- Roest W. R., Verhoef J., & Pilkington M. (1992). Magnetic interpretation using the 3-D analytic signal. *Geophysics*, 57(1), 116-125. <https://doi.org/10.1190/1.1443174>
- Sahoo, S., Narayan, S., & Pal, S. K. (2022a). Fractal analysis of lineaments using CryoSat-2 and Jason-1 satellite-derived gravity data: Evidence of a uniform tectonic activity over the middle part of the Central Indian Ridge. *Phys. Chem. Earth*, 128103237. <https://doi.org/10.1016/j.pce.2022.103237>
- Sahoo, S., Narayan, S., & Pal, S. K. (2022b). Appraisal of gravity-based lineaments around Central Indian Ridge (CIR) in different geological periods: Evidence of frequent ridge jumps in the southern block of CIR. *J. Asian Earth Sci.*, 239105393. <https://doi.org/10.1016/j.jseas.2022.105393>
- Stampolidis, A., & Tsokas, G.N. (2012). Use of edge delineating methods in interpreting magnetic archaeological prospection data. *Archaeological Prospection*, 19(2), 123-140. <https://doi.org/10.1002/arp.1424>
- Verduzco, B., Fairhead, J.D., Green, C.M. & MacKenzie, C. (2004). New insights into magnetic derivatives for structural mapping. *The Leading edge*, 23(2), 116-119. <https://doi.org/10.1190/1.1651454>
- Wijns, C., Perez, C. & Kowalczyk, P. (2005). Theta map: Edge detection in magnetic data. *Geophysics*, 70(4), L39-L43. <https://doi.org/10.1190/1.1988184>
- Yao, Y., Huang, D., Yu, X. & Chai, B. (2016). Edge interpretation of potential field data with the normalized enhanced analytic signal. *Acta Geodaetica et Geophysica*, 51(1), 125-136. <https://doi.org/10.1007/s40328-015-0120-x>
- Zhang, X., Yu, P., Tang, R., Xiang, Y., & Zhao, C. J. (2015). Edge enhancement of potential field data using an enhanced tilt angle. *Exploration Geophysics*, 46(3), 276-283. <https://doi.org/10.1071/EG13104>